

Visual Predictions in the Orbitofrontal Cortex Rely on Associative Content

Maximilien Chaumon^{1,2,3}, Kestutis Kveraga², Lisa Feldman Barrett^{1,2} and Moshe Bar^{2,4}

¹Interdisciplinary Affective Science Laboratory, Department of Psychology, Northeastern University, Boston, MA 02115, USA,

²Athinoula A. Martinos Center for Biomedical Imaging, Massachusetts General Hospital and Harvard Medical School, Charlestown, MA 02129, USA, ³Berlin School of Mind and Brain, Humboldt Universität zu Berlin, Berlin 10117, Germany and ⁴Gonda Center for Brain Research, Bar-Ilan University, Ramat Gan, Israel

Address correspondence to Maximilien Chaumon, Berlin School of Mind and Brain, Luisenstrasse 56, 10117 Berlin, Germany. Email: maximilien.chaumon@gmail.com

Predicting upcoming events from incomplete information is an essential brain function. The orbitofrontal cortex (OFC) plays a critical role in this process by facilitating recognition of sensory inputs via predictive feedback to sensory cortices. In the visual domain, the OFC is engaged by low spatial frequency (LSF) and magnocellular-biased inputs, but beyond this, we know little about the information content required to activate it. Is the OFC automatically engaged to analyze any LSF information for meaning? Or is it engaged only when LSF information matches preexisting memory associations? We tested these hypotheses and show that only LSF information that could be linked to memory associations engages the OFC. Specifically, LSF stimuli activated the OFC in 2 distinct medial and lateral regions only if they resembled known visual objects. More identifiable objects increased activity in the medial OFC, known for its function in affective responses. Furthermore, these objects also increased the connectivity of the lateral OFC with the ventral visual cortex, a crucial region for object identification. At the interface between sensory, memory, and affective processing, the OFC thus appears to be attuned to the associative content of visual information and to play a central role in visuo-affective prediction.

Keywords: fMRI, perception, top-down

Introduction

Visual recognition is shaped by memory and expectations accumulated from lifelong interactions with objects. We are only beginning to understand how those memories facilitate the analysis of visual information, and what brain networks are involved in making use of previous experience when perceiving new stimuli. The orbitofrontal cortex (OFC) appears to have a crucial function in integrating incoming sensory information with memory to facilitate recognition. This study aims to understand the nature of the visual information employed in the OFC to generate early predictions that guide perception and behavior.

Specifically, we test predictions of a model by Bar (2004), who proposed that the OFC receives coarse, partially analyzed information from visual stimuli before an object is actually recognized, and uses this information to generate a “first guess” prediction about the identity of the object. This visual prediction is then back-projected top-down to occipito-temporal visual regions to promote recognition. In line with this model, it is well known that the OFC is activated early in response to visual stimuli in animals (Thorpe et al. 1983; Rolls and Baylis 1994; Rolls et al. 2005, 2006) and in humans (Bar et al. 2006; Chaumon et al. 2009; Gamond et al. 2010). Human electrophysiology and modeling studies have also shown that the first

wave of spikes in the visual system carries enough information to allow reliable guesses as to the identity of the stimulus (Van-Rullen and Thorpe 2001; VanRullen and Koch 2003). In direct support of the model, Bar et al. (2006) showed that the OFC is activated before the higher-order visual regions in the ventral temporal cortex, and that this activity is followed by a period of synchronization between the OFC and the fusiform cortex, suggesting a transfer of information between the 2 regions. Moreover, the OFC is still activated early when only the low spatial frequency (LSF) of a visual object image is presented, supporting the view that a coarse representation of the visual input is enough to generate predictions in the OFC. The fast magnocellular neurons of the visual system, which are most sensitive to LSF, could provide the initial input to projection pathways to the OFC. Although these pathways have not been clearly identified, they could run through the dorsal visual pathway (Livingstone and Hubel 1987; Merigan and Maunsell 1993) and/or through subcortical pathways, possibly via the pulvinar nucleus of the thalamus (Morris et al. 1999). In any case, another study using visual stimuli manipulated to a bias processing toward either the magnocellular or the parvocellular visual pathway showed that the OFC was preferentially activated by magnocellular-biased stimuli (Kveraga et al. 2007), supporting the idea that this cellular type is critical in the rapid activation of the OFC by visual information.

But exactly what type of information carried in the LSF is necessary for the OFC to generate these predictions? Does the OFC attempt to predict the identity of each and every stimulus that activates the visual system? In this case, even the most meaningless LSF information should activate the OFC, and the spatial frequencies in the input would be the critical factor for its activation. Meaningless LSF information such as oriented gratings would thus activate the OFC more than high spatial frequency (HSF)-oriented gratings. Another possibility is that the OFC requires the incoming sensory information to evoke memory associations and to generate predictions as to the identity of the object. In this case, only “meaningful” LSF visual objects should activate the OFC, they would do so to a greater extent than meaningless gratings, and this activation would increase with a measure of stimulus meaningfulness.

This study thus tested the following hypothesis: we evaluated whether meaningful content is required in visual stimuli to activate the OFC. To accomplish this goal, we characterized the dimensions of visual information that activate the OFC to understand how sensory input is transformed in this region. We first conducted a series of measures where separate groups of participants rated LSF-filtered objects for their associative content. These ratings were performed along 2 broad associative domains (identity and affect) to investigate how these

factors influence the activation of OFC. It is worth noting here that we did not mean to assess specific episodic memories, but rather more general semantic knowledge attached to objects presented in canonical orientations (see Discussion). We also measured the low-level visual properties of these stimuli to evaluate whether any of these properties could activate the OFC directly. We then presented these normed objects, along with oriented gratings lacking any type of associations in memory, to a new group of healthy participants in a functional magnetic resonance imaging (fMRI) experiment. This design allowed us to determine how stimulus identity, affective associations, and low-level visual properties affect the activation of the OFC. Finally, although the methodology we used does not allow addressing directly whether the OFC generates predictions (but see Bar 2004; Kveraga et al. 2007, 2011), we used functional connectivity analyses to evaluate whether the OFC communicates with other brain regions during our

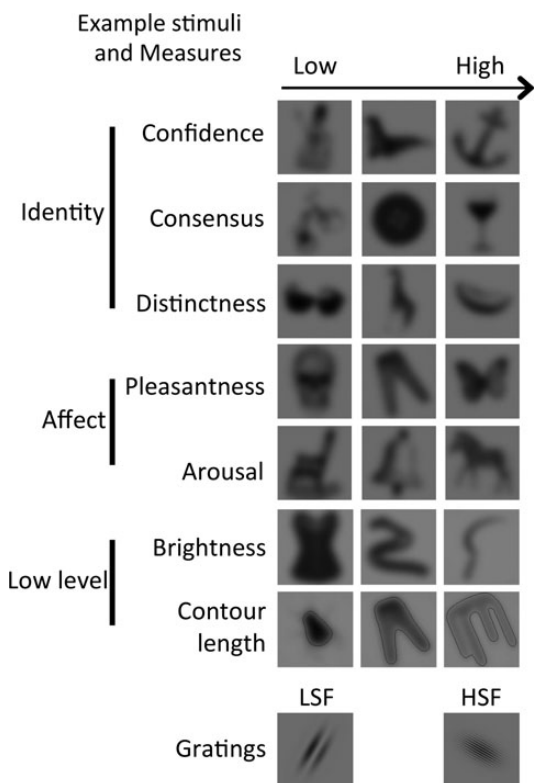


Figure 1. Examples of LSF images and their measures taken along 7 dimensions. Identity measures were confidence, consensus, and distinctness. Affect measures were pleasantness and arousal. Low-level measures were average luminance and contour length. Two exemplar gratings are also shown in the last row.

experimental task. We expected that the OFC would facilitate visual processing in the ventral visual pathway and thus focused on connectivity changes between the OFC and the ventral visual pathway.

Materials and Methods

Behavioral Norming Procedure

A series of 7 measurements was obtained from a separate group of subjects. Images of real objects were low-pass filtered to generate the stimuli (Fig. 1). See Supplementary Material for a detailed description of stimulus generation and procedure.

Descriptive statistics for the 7 stimulus dimensions (confidence, consensus, distinctness, pleasantness, arousal, brightness, and contour length) can be found in Table 1. Three of these measures reflected the identity associations evoked by the images, and how easily they could be retrieved from memory. These dimensions will collectively be referred to as "identity" association measures. Two other measures were indices of the affective value of the images and will collectively be referred to as "affect" association measures. The 2 measures of low-level property metrics are referred to collectively as "low-level" measures. These dimensions were used to create condition regressors in the general linear modeling of the fMRI data.

fMRI Experiment

Participants

Twenty healthy right-handed participants with no reported history of neurological or affective disorders, and normal or corrected-to-normal visual acuity and color discrimination took part in the fMRI experiment. Written informed consent was obtained prior to the start of the scanning session, in accordance with a Human Studies Protocol (#2001P-001754) approved by the Massachusetts General Hospital. All participants were remunerated with 65 USD. None of these participants had performed the norming session described above. Three participants were excluded because they did not complete the scanning session, leaving 17 participants (10 females, age 23–35, mean: 25.6, standard deviation [SD] 3.9) for the group analyses.

Image Acquisition

Images were acquired using a Siemens 3-T Trio Tim MR magnet and a 32-channel radiofrequency head coil. We acquired functional image volumes as T_2^* -weighted echo-planar images (EPIs) with the following parameters: 33 interleaved axial slices, 2000 ms time repetition (TR), 28 ms time echo, 2.5 mm thickness, 0.75 mm gap, 64 × 64 matrix, 200 mm field of view (resulting in an in-plane voxel size of 3.125 × 3.125 × 2.5 mm). Our fMRI sequence and slice prescription were optimized for reducing signal loss and distortion in the OFC (based on recommendations in Deichmann et al. 2003), including the use of a modified z-shim prepulse moment and an anterior 30° tilt of our slice prescription from the anterior commissure/posterior commissure line. Each participant performed 3 functional runs, each consisting of 231 TRs. Each run included 10 s of fixation at the beginning (to allow for the fMRI signal to reach steady-state magnetization), and the

Table 1
Descriptive statistics of the tested measures of the visual stimuli

Measure	Description	Mean	Standard deviation	Range	Range (Z)	Minimum	Maximum
Confidence	Click on a continuous scale frequency of the most	0.49	0.15	0.63	4.33	0.24	0.87
Consensus	Frequency of the most frequency of the most across participants	0.48	0.27	0.92	3.44	0.08	1.00
Distinctness	Inverse of the average number of different labels given by subjects	0.52	0.09	0.56	6.28	0.40	0.96
Pleasantness	Click on a continuous scale	0.54	0.10	0.57	5.76	0.20	0.77
Arousal	Click on a continuous scale	0.51	0.05	0.32	5.74	0.34	0.65
Brightness	Average of the pixel values	0.49	0.00	0.02	5.61	0.48	0.50
Contour length	Length of the contours delineated by the image	0.49	0.13	0.81	6.39	0.19	1.00

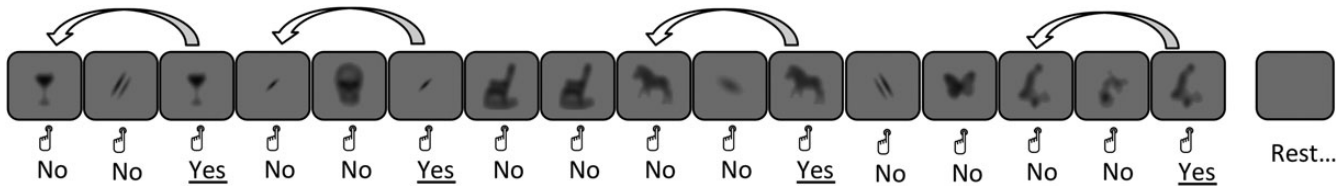


Figure 2. Schematic trial structure of one epoch. Objects and gratings were presented in a mixed pseudorandomized order. Subjects had to press 1 of the 2 buttons in response to each stimulus to indicate whether or not that stimulus was the same as the one presented 2 stimuli before. There were 4–5 such targets per epoch of 16 trials (4 represented here). A resting period of 10 s was presented after each epoch. Thirty-three such epochs were presented to each subject. Only the responses to correct “No” responses to unrepeated stimuli were analyzed. All images were associated with a measure from each of the dimensions presented in Figure 1, which were used as covariates in the general linear model of the data.

first 5 EPI volumes were discarded from further analysis. Each session included the acquisition of 2 high-resolution T_1 -weighted multi-echo magnetization-prepared rapid acquisition with gradient echo (MEMPRAGE) anatomical images (1-mm isotropic voxels), which were later averaged together.

fMRI Task and Procedure

The paradigm employed a rapid event-related design. Figure 2 presents a schematic overview of the task. Participants were presented with the blurred images used in the norming procedure intermixed with gray-oriented gratings in an unpredictable pseudorandom order. We used a 2-back working memory task to ensure that participants paid attention on each trial. Participants had to press one button when the current object was identical to the one presented 2 trials ago, and another button otherwise. The gratings were created by multiplying a 2-dimensional sinusoid with an elongated Gaussian envelope. The sinusoids were either LSF (2 or 3 cpi) or HSF (12 or 18 cpi), randomly oriented in steps of 15° (11 orientations). Objects were darker than the gray background. Similarly, gratings were spanning only darker luminance than the background. The Gaussian envelopes were elongated along the axis of the grating to favor the perception of its orientation, important for performing the 2-back task (see example stimuli in Fig. 1, bottom row).

On a given trial, an image (LSF object or grating) appeared for 250 ms followed by a response period of 1500 ms. A gray screen was presented during the interstimulus interval, lasting 0–500 ms (drawn from a uniform random distribution). Stimulus presentation was thus jittered 500 ms with respect to TR. A small dot appeared in the middle of the screen upon button press to indicate participants that their response was recorded, but no feedback was given with respect to the 2-back task performance. Trials were grouped by epochs of 16. Each epoch began with the word “Ready!” displayed for 1.5 s, followed by 500 ms of gray screen before the first image was presented. Each epoch contained 6 different object images and 4 different gratings. Target events (repetitions of the image presented 2 trials before) occurred 4–5 times per epoch. Foil nontarget repeats (repetitions of the image presented on the previous trial) occurred 1–2 times per epoch to ensure that participants’ responses were based on more than just the fact that the image was presented repeatedly.

Each epoch was followed by a 10-s period, which served as a baseline for data analysis and rest period for the participants. There were 11 epochs in 1 acquisition run and 3 runs per participant.

Data Processing

Structural and functional imaging analyses were performed using the SPM8 analysis software (<http://www.fil.ion.ucl.ac.uk/spm/>). Data from individual fMRI runs were first motion corrected: All images were aligned to the first image of the first functional run. The anatomical volumes were coregistered to the mean functional volume. A normalization transformation was calculated from the coregistered anatomical data to a normalized brain (Montreal Neurological Institute ICBM152) and applied to each functional volume. The data were spatially smoothed using a Gaussian full-width half-maximum kernel of 5 mm. Motion outliers were detected and rejected using the Artifact Detection tools (http://www.nitrc.org/projects/artifact_detect/). Time points at which the global root mean square (RMS) of the signal power across all

voxels deviated from the global average by >3 standard deviations were rejected. Time points at which motion from the preceding time point (translation or rotation in 3 dimensions) >3 mm were rejected. Unique regressors were used to discard each of these time points from the analysis. Motion parameters calculated during the motion correction step were also modeled as separate regressors. The estimated hemodynamic response was defined by a gamma function of 2.25-s hemodynamic delay and 1.25-s dispersion.

Data Analysis

All analyses were performed using the various tools implemented in SPM8 (<http://www.fil.ion.ucl.ac.uk/spm/>), as well as third-party toolboxes, including xjview (<http://www.alivelearn.net/xjview/>), rfxplot (Glässcher 2009), snpm toolbox (<http://go.warwick.ac.uk/tenichols/snmp/>), and mricron (<http://www.mccauslandcenter.sc.edu/mricro/mricron/>).

For statistical testing, we used a nonparametric permutation approach, as implemented in the SnPM toolbox, using 2000 random permutations under the null hypothesis, and $P < 0.05$ family-wise error (FEW) rate correction for multiple comparison. To increase sensitivity in the OFC region, the permutations and tests were computed within a region of interest (ROI) including only the orbital regions of the automated anatomical labeling atlas (Tzourio-Mazoyer et al. 2002): Gyrus rectus, and the orbital part of superior, middle, and inferior frontal gyri. Whole brain permutations were also computed in order to extract regions of the ventral temporal cortex more active in response to LSF images than to gratings (Fig. 3B). These regions were also used to restrict testing in the psychophysiological interaction (PPI) analysis (see below).

In all models, repeated images (i.e. targets and foils) were modeled using a separate regressor later treated as a covariate of no interest. The remaining images and gratings were modeled as separate regressors. Gratings were modeled as 2 regressors, one for LSF gratings and another for HSF gratings.

Two types of models were created as categorical and parametric models. Categorical models used the measures obtained in the norming procedure to split images into 3 separate conditions (at the 33rd and 66th percentiles), modeled via distinct regressors. Activations elicited by each of these separate conditions could then be directly compared with the activation by gratings. In parametric models, images were entered as a single regressor, and the measures obtained in the norming procedure were introduced as parametric modulators over image onset to isolate the effect of each measure on the response to the images. Note that we used both types of models because only the categorical models allowed comparing images of varying intensity along each of the measures with gratings directly, whereas only the parametric models allowed extracting the effect of each measure independently of the occurrence of the gratings. The measures of interest tended to be highly correlated (Table 2 and Results section) and were modeled separately to avoid ambiguity in the interpretation of the results (Andrade et al. 1999).

We also modeled PPIs (Friston et al. 1997). In each of the tested models, the physiological variable was the time course of activity extracted at an ROI, and the psychological variable was one of the measures. This analysis reveals areas whose correlation with the ROI varies as a function of the level of the psychological variable. ROIs

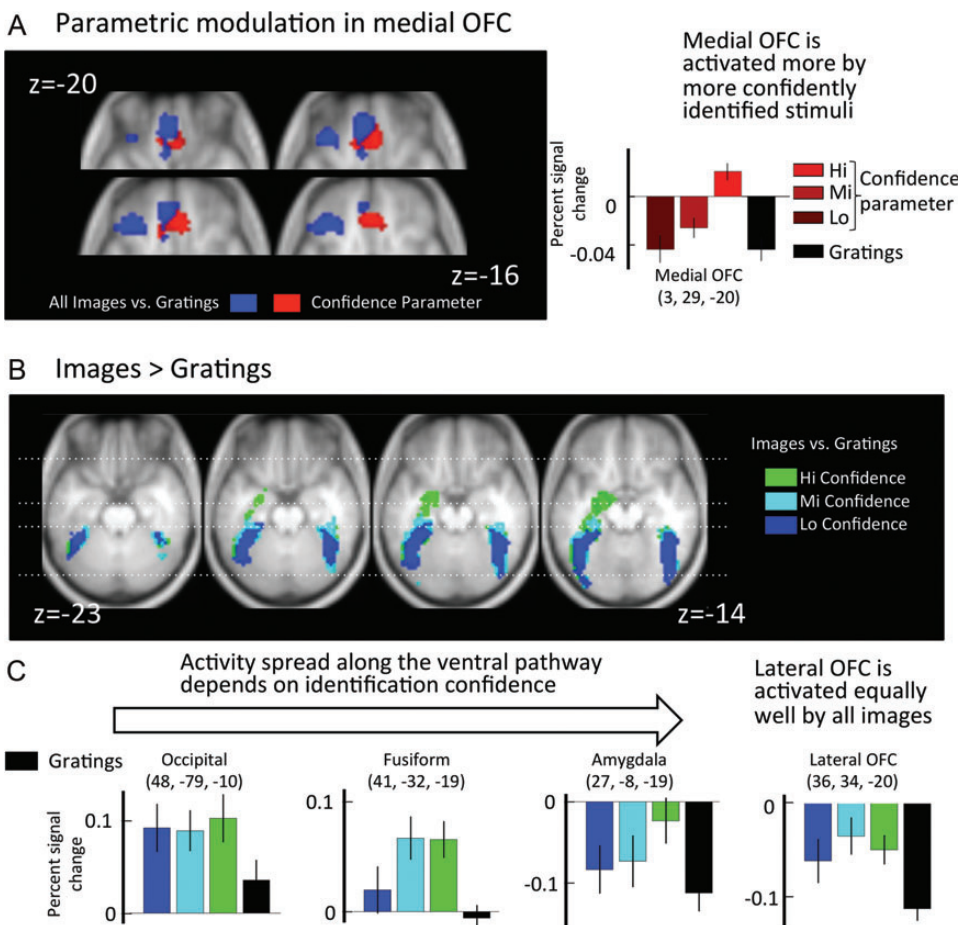


Figure 3. Response pattern of the confidence reactive region in the medial OFC, and whole-brain response to LSF images compared with gratings. (A) Parametric modulation of image response by confidence in the OFC. The effect of the confidence parametric regressor is shown in red, and the overall response to images versus gratings is shown in blue. The bar graph on the right shows activations within the cluster responding to confidence. They are not independent of the isolated contrast cluster and are shown for illustrating the effect. (B) Greater response to LSF images than to gratings. Response of images with low (blue), medium (cyan), and high (green) degrees of confidence are shown in horizontal slices of the average brain anatomy. Z-coordinate increments in steps of 3 mm from left to right. (C) Bar plots showing the response to images compared with rest periods in 4 different regions indicated above each graph. The Y-coordinates of these regions correspond to the thin dotted white lines overlayed on the maps in B. The black bars represent the response to the gratings and the 3 levels of confidence use the same color code as on the brain slices in B. All coordinates are in the Montreal Neurological Institute frame. For all maps, significance was assessed by means of nonparametric permutation statistics corrected for family-wise error rate ($P < 0.05$).

were defined for each participant individually as a 3-mm radius sphere centered at the peak of the images versus gratings contrasts within the OFC, and PPI effects were evaluated within the regions more active in response to images than to gratings in the ventral visual pathway.

Results

Behavioral Norming Procedure

Correlations between all ratings are presented in Table 2. Correlations were strongest among the identity association measures (Confidence, Consensus, and Distinctness), with 12–67% of shared variance (R^2). This indicates that participants were more confident about the identity of the objects when these were distinct from other object categories and could hardly lead to any other categorical interpretation both within and between subjects (high distinctness and high consensus, respectively). As a consequence, it thus seems that the identity association measures quantify the same feature of the stimuli and we will consider them collectively while interpreting the results. Confidence will be used for illustration in the

Table 2
Correlations across measures

	1.00						
Confidence	1.00						
Consensus	0.82	1.00					
Distinctness	0.46	0.67	1.00				
Pleasantness	0.49	0.33	0.23	1.00			
Arousal	0.28	0.27	0.27	0.04	1.00		
Brightness	0.09	0.12	0.07	-0.01	0.03	1.00	
Contour	-0.01	-0.03	-0.08	0.07	-0.15	-0.25	1.00

Note: Pearson's r correlation coefficient is shown. Significant correlations are on a gray background (darker gray $P < 0.001$, lighter gray $P < 0.05$).

remainder of this study, but all the identity association measures showed qualitatively similar results (as shown in Supplementary Fig. 1).

The affect association measures were not correlated with each other, in line with reports that these 2 core dimensions of affect are orthogonal measures (Russell and Barrett 1999). These measures were moderately correlated with the identity association measures: In particular, Confidence and Pleasantness measures shared 24% of variance. Concerning low-level nonassociative image properties, brightness and contour

length correlated with each other, but not with any other measure (all $|r| \leq 0.15$). These correlations indicate that participants found those objects that they identified with more confidence generally more pleasant. This is in line with earlier findings showing that more familiar objects are generally perceived as more pleasant than novel ones (Zajonc 1968).

fMRI Experiment

Behavior

Participants performed well above chance on the 2-back task ($d' = 2.53 \pm 0.17$ SEM), but had a higher sensitivity for real object images ($d' = 2.77$) than for gratings ($d' = 2.31$, 2-tailed paired t -test: $t_{(16)} = 4.23$, $P < 0.001$). This was due to a lower false alarm rate for objects (0.04) than for gratings (0.07; $t_{(16)} = 4.16$, $P < 0.001$). The hit rate on the other hand was not different between objects and gratings ($t_{(16)} = 1.15$, n.s.). Reaction times were also shorter for images (mean = 670 ms, SEM = 20 ms) than for gratings (mean = 700 ms, SEM = 25 ms; $t_{(16)} = 3.40$, $P < 0.005$).

Participants were also more likely to detect 2-back repeats for highly identifiable images than for the least identifiable images. Categorizing behavioral performance based on the ratings in the identity association measures (lowest 33% vs. highest 33% rated images), we found a significant difference in hit rates between the high and low measures of confidence ($t_{(16)} = 4.96$, $P < 0.001$), consensus ($t_{(16)} = 5.25$, $P < 0.0001$), and distinctness ($t_{(16)} = 3.37$, $P < 0.005$). No significant effect was found on false alarm rates. The affect association measures had no effect on performance. All the participants reported trying to identify the objects during the experiment, just as they were encouraged to do in the task instructions.

In summary, identifying objects facilitated detecting repetitions, as shown by enhanced performance for objects

compared with gratings, and for more identifiable objects versus less identifiable objects.

Neuroimaging

As predicted, regions of the occipital cortex, but not of the OFC, responded to HSF and LSF gratings. The effect of the spatial frequency of the gratings at the whole-brain level was confined to the occipital lobe and barely spread outside of the low-level visual areas. The HSF versus LSF contrast for gratings showed positive activation in early visual areas at the occipital pole and a posterior region of the fusiform gyrus. Statistical testing restricted to the OFC revealed no effect in that region.

In contrast, LSF images of visual objects preferentially increased the activation in 2 clusters within the OFC compared with gratings (Fig. 3A). One cluster was situated medially in the gyrus rectus (approximately corresponding to Brodmann's Area (BA) 11 and 14) and the other cluster was located on the left, in the lateral OFC (approximately in BA 47/12m, as defined by Öngür et al. 2003). Note that a symmetrical region on the right also seemed to respond more to images than to gratings, but failed to reach significance.

At the whole-brain level, the contrast between LSF images and gratings revealed 2 large clusters, shown in Figure 3B and described in Table 3. We restricted testing to these clusters to examine how increasing the level of confidence affected activity in the ventral visual pathway. This analysis reveals that the spread of activity along the ventral visual pathway increased for images that were identified with more confidence (Fig. 3B). As shown in the bar graphs of Figure 3C, all images activated the most posterior regions of the ventral visual pathway. More anteriorly, in the fusiform gyrus, only moderately and highly confidently identified images triggered more activity than gratings. Finally, the most anterior regions of the ventral pathway and the amygdala were only activated by the

Table 3

List of all activations found in this study

Contrast	ROI	Cluster #	Voxel		Cluster Number of voxels	P(FWE correction)	Peak MNI coordinates			
			P(FWE correction)	Peak intensity (T)			x	y	z	region
Images > gratings	Whole brain	1	0.0005	11.50	967	0.0180	42	-82	-8	right lateral occipital through ventral pathway
		2	0.0015	9.29	1021	0.0165	-42	82	-2	left lateral occipital through the ventral pathway
	OFC	1	0.0005	7.96	172	0.0160	-36	35	-14	Left OFC
		2	0.0055	6.45	161	0.0180	-6	44	-20	Medial OFC
Gratings > images	Whole brain	1	0.0005	9.61	2040	0.0035	9	-88	-2	bilateral medial posterior occipital cortex
		2	0.0010	9.44	694	0.0345	36	14	49	right middle frontal gyrus
		3	0.0105	7.46	2432	0.0025	39	-64	52	bilateral superior parietal cortex
	OFC	None								
Parametric confidence	Whole brain	None								
	OFC	1	0.0120	5.82	161	0.0045	3	29	-20	Medial OFC
Low confidence images	Images > gratings	1	0.0005	9.59	672	0.0010	42	-82	-5	Right ventral pathway
		2	0.0005	7.58	606	0.0020	-42	-85	-5	Left ventral pathway
Mid confidence images	Images > gratings	1	0.0005	10.59	781	0.0005	42	-82	-8	Right ventral pathway
		2	0.0005	9.35	749	0.0010	-42	-85	-2	Left ventral pathway
High confidence images	Images > gratings	1	0.0005	10.25	810	0.0005	42	-82	-8	Right ventral pathway
		2	0.0005	8.96	890	0.0005	-33	-40	-20	Left ventral pathway
PPI right OFC	Whole brain	None								
	Images > gratings	1	0.0325	4.98	333	0.0015	51	-64	-8	Posterior right ventral pathway
PPI left OFC	Whole brain	None								
	Images > gratings	1	0.0185	5.44	225	0.0020	36	-49	-14	Posterior right ventral pathway
		2	0.1190	4.30	133	0.0090	-42	-79	-5	Posterior left ventral pathway

Note: Only clusters with a corrected P -value < 0.05 within the considered ROI (statistical mask) are shown. Each of the horizontally separated sections shows results from a different general linear model design.

images identified with most confidence (similar effects were observed in the left hemisphere, but are not shown). Strikingly, all the images, including the least confidently identified ones, activated the OFC in the lateral cluster described above. In this part of the figure, data are extracted from spherical ROIs 6 mm in diameter spaced along the ventral temporal cortex, centered within the regions activated by the most confidently identified objects (in green throughout Fig. 3). Percent signal change is calculated with respect to the average activity (beta weight of the session constant regressors) in each region, as computed by the rxplot software (Gläscher 2009). A similar spread of activity was also found for the other identity and affect measures (Supplementary Fig. 1).

The medial OFC is responsive to all the LSF images of objects, but, as is shown in Figure 3A, the extent of this activation seems to vary with the level of identification confidence evoked by the images. To verify this and to isolate the areas specifically sensitive to the level of each of the association measures, we defined separate models, each using one association measure as a continuous parametric regressor in addition to a regressor of no interest for the onset of all the images. We tested these parametric models within the OFC and revealed a significant effect for the confidence measure in the medial OFC. It is worth noting that the contrasts performed with the categorical and parametric models were not sensitive to the same partition of total variance: The contrasts in the categorical models compared activation by gratings with response to images, whereas the gratings were modeled with regressors of no interest in the parametric models. The results from the 2 models are thus not directly comparable, but rather provide complimentary information. Categorical models provide information as to the difference between LSF images and gratings, whereas the parametric models reveal a pure effect of the associative measures. This is illustrated in Figure 3A, and activations for the parametric modulation are listed in Table 3. Other identity measures (consensus and distinctness) showed only marginal effects that failed to reach our significance criterion. Affect measures failed to show any effect in the OFC. Maps showing the effects for all measures with a less-stringent correction for multiple comparisons (classical *t*-statistics, $P < 0.05$, minimal cluster size of 20 voxels) are shown in Supplementary Material for information.

To further illustrate how identification confidence influences OFC activity, the bar plot in Figure 3A illustrates the response pattern to the confidence parameter in the medial OFC region, extracted in a nonindependent way from the significant region highlighted in red in the left part of the figure. The largest deviation from the response to the gratings appeared in response to images with the highest levels of identity measures, and the smallest deviation for images with lowest levels of identity measures. We know that qualitative differences might exist in the physiological response to stimuli with different affective properties in the prefrontal cortex. These might involve different neurotransmitters with different receptor subtypes, having vasoactive properties that interact in a nonlinear and sometimes counteracting manner (Choi et al. 2006), leading to a nontrivial interpretation of blood oxygen level dependent (BOLD) signal decreases in terms of neuronal activity (Harel et al. 2002; Vanzetta and Slovin 2010). Nevertheless, in the present case, it still seems likely that the similarity in the BOLD response to completely meaningless gratings and stimuli to which hardly any meaning could be attributed reflects a similarity in the underlying neural processes.

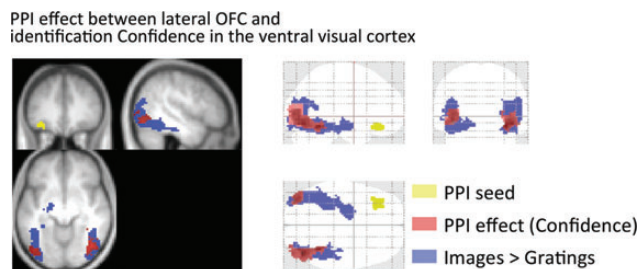


Figure 4. PPI effects between the lateral OFC region, confidence, and activity in regions more active in response to images than to gratings. Left: significant PPI regions (red) for the lateral OFC ROI (yellow) within the regions more active in response to images than to gratings (blue). Effects are displayed on the average structural brain on 3 orthogonal slices centered at coordinates: $x = 48$, $y = 36$, $z = -9$. Right: Same as left, but displayed on a transparent glassbrain. For all maps, testing was restricted to the regions significantly more active in response to LSF images than to gratings. Significance was assessed by means of nonparametric permutation statistics corrected for family-wise error rate ($P < 0.05$).

To control for potential confounds in the above results, we also analyzed models in which low-level nonassociative features of the images were modeled separately. We found no effect of these properties when restricting the analysis to the OFC. The brightness of the images tended to activate regions of the occipital lobe, and contour length tended to activate more anterior areas in the medio-ventral visual pathway, along the fusiform gyrus, but whole-brain analysis failed to reach significance. These activations are documented for information on Supplementary Material (Supplementary Fig. 2).

Finally, the correlation of activity between the lateral OFC and the ventral visual pathway depended on the amount of identity associations evoked by the images. We performed an PPI analysis to see how each of the measures affected the correlation between areas more active in response to LSF images than to gratings, and the ventral visual pathway regions more active in response to images than to gratings (Fig. 4). The seed regions for this PPI analysis were taken at the peak of the activations responding more to LSF images of objects than to gratings found within the lateral and medial OFC in each participant. Only the lateral OFC region revealed a significant PPI effect with the ventral visual pathway. In agreement with our hypothesis, the more confidently identified images strengthened functional connectivity between the lateral OFC region and the posterior regions of the ventral visual pathway. Among the voxels that responded more strongly to images than to gratings, 18% also showed a PPI effect. These voxels were essentially located in posterior regions, as shown in Figure 4, suggesting that activity in some of the voxels that were most connected with the lateral OFC regions was also participating to the visual analysis of the LSF images. The more confidently identified images positively affected correlation between the left OFC and large regions of the left and right fusiform gyri extending into the middle occipital gyrus on the right. In contrast, none of the affective or low-level measures affected correlation between the lateral OFC and posterior cortices. None of the measures affected the correlation between the medial OFC cluster and any posterior cortices.

Discussion

The OFC is known to respond preferentially to LSF compared with HSF visual information during visual recognition. We

demonstrate here that this response preference depends on the identifiability of the visual stimuli: While meaningless gratings of varying spatial frequencies do not activate the OFC differentially, LSF pictures of real-world objects clearly do. Critically, the degree of identifiability of these meaningful stimuli modulates activity in the medial OFC and the functional connectivity between the lateral OFC and the ventral visual pathway. This study thus reveals a fundamental condition under which visual information activates the OFC, thus contributing to our understanding of how the OFC facilitates vision.

Previous research had already revealed that the OFC plays a role in visual performance, but the actual visual dimensions to which it is sensitive remained unexplored. Visual responses in the OFC were reported to be highly specific to certain types of stimuli (Thorpe et al. 1983) and to specific visual categories, such as faces (Ó Scalaidhe et al. 1997; Ishai et al. 2005; Rolls et al. 2006), or novel objects (Rolls et al. 2005). Lesions to the OFC also directly impair recognition and memory for objects (Bachevalier and Mishkin 1986; Kowalska et al. 1991; Meunier et al. 1997). Some studies directly implicated the OFC in the process of visual recognition (Bar et al. 2001; Ishai et al. 2005; Pourtois et al. 2009) and determined that it responds to LSF-filtered visual images (Bar et al. 2006) and images biased to activate the magnocellular neurons of the visual system (Kveraga et al. 2007). But none had examined whether associative and nonassociative dimensions of the visual stimulus, or even completely meaningless gratings could activate the OFC. Our results clarify this issue, showing that only stimuli resembling known objects, and thus activating semantic associations, trigger a response in the OFC.

What happens in the OFC once it is activated? What is the impact of this activation? This question is crucial to understand the functional significance of the visual sensitivity of the OFC found here. Although our results support the idea that OFC provides a predictive signal to the visual system, other methodologies with higher temporal resolution would be needed to assert the causal influence on ventral-temporal areas with sufficient resolution. We thus cannot provide a definite answer, but our findings suggest an interesting possibility. We proposed that the generation of predictions in the OFC promotes recognition, which requires processing along the ventral pathway. Here, we showed that it is only when objects were highly identifiable that visual activity spread all the way up the ventral visual pathway (Fig. 3A). In addition, we showed that these highly identifiable objects triggered a higher correlation between the lateral OFC and the ventral visual cortex (Fig. 4). This result thus opens the possibility that the top-down predictions sent by the OFC gate the activation of the ventral visual pathway. In other words, activating semantic information in the OFC biases low-level visual information processing via feedback loops, so that representations well matched to memory associations in the OFC are strengthened in the ventral visual pathway, facilitating their recognition. This idea is reminiscent of the predictive coding hypothesis (Rao and Ballard 1999) and in line with our model of visual recognition (Bar 2004).

What is the function of the medial and lateral regions that we isolated? The OFC is a complex ensemble of areas and it is becoming increasingly clear that this rather large swath of the cortex does not play just a single role in cognition (Kringelbach and Rolls 2004; Wallis 2012; Walton et al. 2011). In this context, the medial and lateral regions of OFC found here

might be part of 2 systems, jointly activated by the LSF stimuli, but having different functions. The known anatomy of the OFC supports this hypothesis. Indeed, at least 2 networks of interconnected areas exist within the OFC. On the one hand, the medial network includes areas of the ventro-medial surface of the frontal lobe, and 2 caudolateral regions. It is connected with major autonomic bodily control centers, with the limbic system, and reward centers in the ventro-medial caudate and putamen (Barbas and Blatt 1995; Carmichael and Price 1995; Öngür and Price 2000; Saleem et al. 2008). On the other hand, the orbital network includes areas from the central and lateral part of the orbital cortex (Price et al. 1996; Öngür and Price 2000; Saleem et al. 2008) and receives input from all the sensory systems via its extensive bidirectional connections with the sensory processing streams (Price et al. 1996; Rolls 2000; Petrides and Pandya 2002; Carmichael and Price 2004). The 2 subregions we found in the present study likely belong to each of these 2 networks. The medial cluster, more active in response to objects than to gratings, as well as to more identifiable objects, seems to be part of the medial network. The lateral clusters, more active in response to objects than to gratings, and functionally connected to the ventral visual cortex, seem to be part of the orbital network. In light of the connectivity of the 2 networks, we suggest that the medial OFC region participates in computing the value of the stimuli and communicating this value to the body to prepare an appropriate reaction to the visual information, as well as to the lateral regions of the OFC that could participate in computing and sending the visual predictions to the visual system. Interestingly, this reasoning is in line with recent work in monkeys, showing that neighboring areas 11 and 13, also in the orbital network (Saleem et al. 2008), participate in assigning the value to sensory events (Noonan et al. 2010; Walton et al. 2011).

In line with this view, in a recent extension of our model, Barrett and Bar (2009) proposed that 2 types of predictions are generated in the OFC. Predictions about the identity of the stimulus influence the recognition process proper, while affective predictions initiate the appropriate bodily reaction to the stimulus. In a recent study from our group, we show that the response of the OFC to affective and associative information activates the same region as in this experiment in the medial OFC (Shenhav et al. 2013). However, in the context of the present 2-back working memory task, no direct response to the explicitly measured affective dimension of the objects could be isolated. We nevertheless note that participants had to memorize all stimuli (affective or not) and to perform the task, thus making the pleasantness or arousal elicited by the presented stimulus irrelevant to them. Furthermore, the stimuli used were highly blurred gray-scale images that lacked the realism required to induce an affective response. On the other hand, identifying a stimulus was in itself valuable, because it facilitates categorizing it and manipulating it in working memory. Therefore, it seems that the identifiability measures we employed, rather than the direct measures of pleasantness and arousal, were probably a good proxy to capture the value of the presented objects in this task. In line with recent findings (O'Doherty et al. 2003; Padoa-Schioppa and Assad 2006; Lebreton et al. 2009), we thus interpret the medial OFC response as predominantly affective in nature and suggest that it participates in the generation of visuo-affective predictions.

It is important to note that we are referring to semantic rather than episodic memory associations in this study. In

other words, we assume that the participants in our experiment likely recognized generic semantic (e.g. "this shape looks like a coffee cup"), rather than specific episodic items (e.g. "this shape looks like the coffee cup I bought last year in a souvenir shop in Central Park"). Indeed, we presented most of the objects under canonical viewing conditions, and participants were encouraged to simply name the objects in their mind, rather than recalling any specific object they knew. Even if it is plausible that some participants occasionally associated some of the presented objects to a specific object in their life, it is more likely that, on most of the occasions, they simply recalled a generic concept associated with the presented stimulus. Interestingly, recent studies have showed that the OFC is important to perform a model-based inference on the value of sensory events (e.g. "I like coffee cups"), rather than to retrieve this value from specific past events cached in memory (e.g. "I like this coffee cup"; Schoenbaum and Esber 2010; McDannald et al. 2011; Jones et al. 2012). In light of these recent findings, it will be important to address specifically the issue of whether ambiguous objects associated with semantic or episodic memories are more likely to activate the OFC. In any case, our findings suggest that the OFC does not react to just any type of visual stimulation, but rather than it combines sensory information with semantic associative memory representations. Our results thus support our view that the OFC participates in the identification of visual objects based on associative knowledge.

In conclusion, we found that visual objects bearing meaningful associations activate the OFC, whereas mere visual stimulation without any meaningful associations with an identity memory cannot activate the OFC. We found distinct OFC regions sensitive to visual identity information. In line with our proposal that the OFC facilitates visual recognition by sending top-down predictions about the identity of visual objects, more identifiable stimuli increase the level of correlation between the lateral OFC and the ventral visual pathway. This study thus strengthens the proposed role of the OFC in visual recognition and further specifies how information pertaining to associative knowledge about objects is integrated during visual recognition.

Supplementary Material

Supplementary material can be found at: <http://www.cercor.oxfordjournals.org/>.

Funding

This work was supported by the National Institutes of Health (DP1OD003312 to L.F.B.), National Institute of Mental Health (K01MH084011 to K.K.), National Eye Institute (NEI 1R01EY019477-01 to M.B.), Defense Advanced Research Projects Agency (N10AP20036 to M.B.), and National Science Foundation (NSF BCS-0842947 to M.B.).

Notes

Conflict of Interest: None declared.

References

- Andrade A, Paradis AL, Rouquette S, Poline JB. 1999. Ambiguous results in functional neuroimaging data analysis due to covariate correlation. *NeuroImage*. 10:483–486.
- Bachevalier J, Mishkin M. 1986. Visual recognition impairment follows ventromedial but not dorsolateral prefrontal lesions in monkeys. *Behav Brain Res*. 20:249–261.
- Bar M. 2004. Visual objects in context. *Nat Rev Neurosci*. 5:617–629.
- Bar M, Kassam K, Ghuman A, Boshyan J, Schmid A, Dale A, Häämäläinen M, Marinkovic K, Schacter D, Rosen BR. 2006. Top-down facilitation of visual recognition. *Proc Natl Acad Sci*. 103:449.
- Bar M, Tootell RBH, Schacter DL, Greve DN, Fischl B, Mendola JD, Rosen BR, Dale AM. 2001. Cortical mechanisms specific to explicit visual object recognition. *Neuron*. 29:529–535.
- Barbas H, Blatt GJ. 1995. Topographically specific hippocampal projections target functionally distinct prefrontal areas in the rhesus monkey. *Hippocampus*. 5:511–533.
- Barrett LF, Bar M. 2009. See it with feeling: affective predictions during object perception. *Philos Trans Roy Soc B*. 364:1325–1334.
- Carmichael ST, Price JL. 1995. Limbic connections of the orbital and medial prefrontal cortex in macaque monkeys. *J Comp Neurol*. 363:615–641.
- Carmichael ST, Price JL. 2004. Sensory and premotor connections of the orbital and medial prefrontal cortex of macaque monkeys. *J Comp Neurol*. 363:642–664.
- Chaumon M, Hasboun D, Baulac M, Adam C, Tallon-Baudry C. 2009. Unconscious contextual memory affects early responses in the anterior temporal lobe. *Brain Res*. 1285:77–87.
- Choi J-K, Chen YI, Hamel E, Jenkins BG. 2006. Brain hemodynamic changes mediated by dopamine receptors: role of the cerebral microvasculature in dopamine-mediated neurovascular coupling. *NeuroImage*. 30:700–712.
- Deichmann R, Gottfried JA, Hutton C, Turner R. 2003. Optimized EPI for fMRI studies of the orbitofrontal cortex. *NeuroImage*. 19:430–441.
- Friston KJ, Buechel C, Fink GR, Morris J, Rolls ET, Dolan RJ. 1997. Psychophysiological and modulatory interactions in neuroimaging. *NeuroImage*. 6:218–229.
- Gamond L, George N, Lemaréchal J-D, Hugueville L, Adam C, Tallon-Baudry C. 2010. Early influence of prior experience on face perception. *NeuroImage*. 54:1415–1426.
- Gläscher J. 2009. Visualization of group inference data in functional neuroimaging. *Neuroinformatics*. 7:73–82.
- Harel N, Lee S-P, Nagaoka T, Kim D-S, Kim S-G. 2002. Origin of negative blood oxygenation level-dependent fMRI signals. *J Cereb Blood Flow Metab*. 22:908–917.
- Ishai A, Schmidt CF, Boesiger P. 2005. Face perception is mediated by a distributed cortical network. *Brain Res Bull*. 67:87–93.
- Jones JL, Esber GR, McDannald MA, Gruber AJ, Hernandez A, Mirenzi A, Schoenbaum G. 2012. Orbitofrontal cortex supports behavior and learning using inferred but not cached values. *Science*. 338:953–956.
- Kowalska DM, Bachevalier J, Mishkin M. 1991. The role of the inferior prefrontal convexity in performance of delayed nonmatching-to-sample. *Neuropsychologia*. 29:583–600.
- Kringelbach ML, Rolls ET. 2004. The functional neuroanatomy of the human orbitofrontal cortex: evidence from neuroimaging and neuropsychology. *Prog Neurobiol*. 72:341–372.
- Kveraga K, Boshyan J, Bar M. 2007. Magnocellular projections as the trigger of top-down facilitation in recognition. *J Neurosci*. 27:1323.
- Kveraga K, Ghuman aS, Kassam KS, Aminoff E, Hamalainen MS, Chaumon M, Bar M. 2011. Early onset of neural synchronization in the contextual associations network. *Proc Natl Acad Sci*. 108:3389–3394.
- Lebreton M, Jorge S, Michel V, Thirion B, Pessiglione M. 2009. An automatic valuation system in the human brain: evidence from functional neuroimaging. *Neuron*. 64:431–439.
- Livingstone MS, Hubel DH. 1987. Psychophysical evidence for separate channels for the perception of form, color, movement, and depth. *J Neurosci*. 7:3416–3468.
- McDannald MA, Lucantonio F, Burke KA, Niv Y, Schoenbaum G. 2011. Ventral striatum and orbitofrontal cortex are both required for model-based, but not model-free, reinforcement learning. *J Neurosci*. 31:2700–2705.

- Merigan WH, Maunsell JHR. 1993. How parallel are the primate visual pathways? *Ann Rev Neurosci.* 16:369–402.
- Meunier M, Bachevalier J, Mishkin M. 1997. Effects of orbital frontal and anterior cingulate lesions on object and spatial memory in rhesus monkeys. *Neuropsychologia.* 35:999–1015.
- Morris JS, Öhman A, Dolan RJ. 1999. A subcortical pathway to the right amygdala mediating “unseen” fear. *Proc Natl Acad Sci USA.* 96:1680–1685.
- Noonan MP, Walton ME, Behrens TEJ, Sallet J, Buckley MJ, Rushworth MFS. 2010. Separate value comparison and learning mechanisms in macaque medial and lateral orbitofrontal cortex. *Proc Natl Acad Sci USA.* 107:20547–20552.
- O'Doherty JP, Winston J, Critchley H, Perrett D, Burt D, Dolan R. 2003. Beauty in a smile: the role of medial orbitofrontal cortex in facial attractiveness. *Neuropsychologia.* 41:147–155.
- Öngür D, Ferry AT, Price JL. 2003. Architectonic subdivision of the human orbital and medial prefrontal cortex. *J Comp Neurol.* 460:425–449.
- Öngür D, Price JL. 2000. The organization of networks within the orbital and medial prefrontal cortex of rats, monkeys and humans. *Cereb Cortex.* 10:206–219.
- Ó'Scalaidhe SP, Wilson FAW, Goldman-Rakic PS. 1997. Areal segregation of face-processing neurons in prefrontal cortex. *Science.* 278:1135–1138.
- Padoa-Schioppa C, Assad JA. 2006. Neurons in the orbitofrontal cortex encode economic value. *Nature.* 441:223–226.
- Petrides M, Pandya DN. 2002. Comparative cytoarchitectonic analysis of the human and the macaque ventrolateral prefrontal cortex and corticocortical connection patterns in the monkey. *Eur J Neurosci.* 16:291–310.
- Pourtois G, Schwartz S, Spiridon M, Martuzzi R, Vuilleumier P. 2009. Object representations for multiple visual categories overlap in lateral occipital and medial fusiform cortex. *Cerebr Cortex.* 19:1806–1819.
- Price JL, Carmichael ST, Drevets WC. 1996. Networks related to the orbital and medial prefrontal cortex: a substrate for emotional behavior? In: G. Holstege RB and CBS, editors. *Progress in Brain Research.* Elsevier. p. 523–536.
- Rao RPN, Ballard D. 1999. Predictive coding in the visual cortex: a functional interpretation of some extra-classical receptive-field effects. *Nat Neurosci.* 2:79–87.
- Rolls E, Baylis L. 1994. Gustatory, olfactory, and visual convergence within the primate orbitofrontal cortex. *J Neurosci.* 14:5437–5452.
- Rolls ET. 2000. The orbitofrontal cortex and reward. *Cerebr Cortex.* 10:284.
- Rolls ET, Browning AS, Inoue K, Hernadi I. 2005. Novel visual stimuli activate a population of neurons in the primate orbitofrontal cortex. *Neurobiol Learn Mem.* 84:111–123.
- Rolls ET, Critchley HD, Browning AS, Inoue K. 2006. Face-selective and auditory neurons in the primate orbitofrontal cortex. *Exp Brain Res.* 170:74–87.
- Russell JA, Barrett LF. 1999. Core affect, prototypical emotional episodes, and other things called “emotion”: dissecting the elephant. *J Pers Soc Psychol.* 76:805.
- Saleem KS, Kondo H, Price JL. 2008. Complementary circuits connecting the orbital and medial prefrontal networks with the temporal, insular, and opercular cortex in the macaque monkey. *J Comp Neurol.* 506:659–693.
- Schoenbaum G, Esber GR. 2010. How do you (estimate you will) like them apples? Integration as a defining trait of orbitofrontal function. *Curr Opin Neurobiol.* 20:205–211.
- Shenhav A, Barrett LF, Bar M. 2013. Affective value and associative processing share a cortical substrate. *Cogn Affect Behav Neurosci.* 13:46–59.
- Thorpe SJ, Rolls ET, Maddison S. 1983. The orbitofrontal cortex: neuronal activity in the behaving monkey. *Exp Brain Res.* 49:93–115.
- Tzourio-Mazoyer N, Landeau B, Papathanassiou D, Crivello F, Etard O, Delcroix N, Mazoyer B, Joliot M. 2002. Automated anatomical labeling of activations in SPM using a macroscopic anatomical parcellation of the MNI MRI single-subject brain. *NeuroImage.* 15:273–289.
- VanRullen R, Koch C. 2003. Visual selective behavior can be triggered by a feed-forward process. *J Cogn Neurosci.* 15:209–217.
- VanRullen R, Thorpe SJ. 2001. Rate coding versus temporal order coding: what the retinal ganglion cells tell the visual cortex. *Neural Comp.* 13:1255–1283.
- Vanzetta I, Slovin H. 2010. A BOLD assumption. *Front Neuroenergetics.* 2:1–4.
- Wallis JD. 2012. Cross-species studies of orbitofrontal cortex and value-based decision-making. *Nat Neurosci.* 15:13–19.
- Walton ME, Behrens TEJ, Noonan MP, Rushworth MFS. 2011. Giving credit where credit is due: orbitofrontal cortex and valuation in an uncertain world. *Ann N Y Acad Sci.* 1239:14–24.
- Zajonc RB. 1968. Attitudinal effects of mere exposure. *J Pers Soc Psychol.* 9:1–27.